



NUMERICAL INVESTIGATION ON THE INFLUENCE OF INTERNAL CAROTID ARTERY GEOMETRY ON WALL SHEAR STRESS DISTRIBUTION

Jianqing FENG¹, Yanbo LIANG², Yan CHEN³, Marie OSHIMA⁴

¹ Department of Mechanical Engineering, Graduate School of Engineering, The University of Tokyo, 7-3-1 Hongo, Bunkyo-ku, Tokyo, Japan. Tel.: +81 080 3448 6133, E-mail: fjq@iis.u-tokyo.ac.jp

² Department of Mechanical Engineering, Graduate School of Engineering, The University of Tokyo. E-mail: liangyanbo00@gmail.com

³ Interfaculty Initiative in Information Studies, The University of Tokyo. E-mail: marie@iis.u-tokyo.ac.jp

⁴ Interfaculty Initiative in Information Studies, The University of Tokyo. E-mail: chenyan@iis.u-tokyo.ac.jp

ABSTRACT

The internal carotid artery (ICA) is the primary blood supply to the brain and exhibits complex geometric variations that influence hemodynamic behavior. In particular, the highly curved siphon region is associated with elevated wall shear stress (WSS), which may cause damage to endothelial cells and contribute to disease progression. However, the quantitative relationship between ICA morphology and WSS distribution remains unclear. To clarify this relationship, we developed a novel ICA centerline classification method based on spatial geometric features and categorized the centerlines extracted from the BraVa dataset into four types: U, V, C, and S. Computational fluid dynamics (CFD) simulations were then conducted to analyze the WSS distribution in each classified geometry and to reveal differences in flow patterns. The results show that the U-type has two high-curvature regions, causing large WSS variations. The V-type has concentrated curvature, leading to a localized high WSS region. C-type torsion and non-coplanar bends create a complex WSS distribution. The S-type resembles the U-type but has a larger B2 bending angle, resulting in higher WSS. These findings highlight the impact of vascular morphology on WSS and support further studies on ICA hemodynamics.

Keywords: Blood flow simulation, geometric classification, internal carotid artery, vascular geometry, wall shear stress

NOMENCLATURE

p	[Pa]	pressure
u	[m/s]	velocity
α	[°]	binormal angle
ν	[m ² /s]	kinematic viscosity
ρ	[kg/m ³]	fluid density
θ	[°]	bend angle

1. INTRODUCTION

Cerebrovascular diseases are a leading cause of death worldwide [1], with aneurysms presenting a significant risk due to their potential for rupture, which can lead to severe complications or fatal outcomes [2]. Therefore, early diagnosis and predictive systems are essential for improving patient prognosis and reducing healthcare costs.

The supraclinoid segment of the ICA is a common site for aneurysm formation, and its complex vascular structures pose challenges for treatment [3]. Understanding the relationship between ICA geometry and hemodynamics is essential for early prediction and non-invasive diagnosis, which can be further advanced through CFD simulations.

The formation of aneurysms is influenced by both hemodynamic forces and vascular geometry. Among these, WSS plays a critical role in aneurysm initiation.[4, 5] High WSS and high WSS gradients contribute to media thinning and bulge formation, marking the early stages of aneurysm development. Furthermore, abnormal WSS induces cell apoptosis, extracellular matrix degradation, and inflammation, accelerating aneurysm progression. Vascular geometry directly affects local hemodynamics; studies on ICA curvature have shown that high-curvature regions are subject to elevated WSS and WSS gradients, increasing their susceptibility to aneurysm formation.[6]

To further refine aneurysm risk assessment, classification methods based on vascular geometry have been explored. Zhang's study [7] categorized ICA into U, V, C, and S types, revealing that vascular shape is associated with disease-related hemodynamic patterns. Sangalli et al.[8] analyzed 65 subjects and found that 70% of ICAs with aneurysms located at or beyond the terminal bifurcation were V-type, whereas all ICAs without aneurysms were U-type. These findings suggest that ICA shape classification may serve as an important indicator of in-

tracranial aneurysm risk and its underlying hemodynamic mechanisms.

However, existing classification methods heavily rely on manual segmentation by medical experts, making them highly subjective and difficult to standardize. Such subjectivity may affect the reliability of comparing WSS distributions among different morphological types. To overcome this limitation, our research group has been developing a novel ICA classification method that utilizes shape features of the vessel centerline to objectively classify ICA geometry, dividing it systematically into new U, V, C, and S types. This approach aims to eliminate subjective biases and improve consistency in vascular shape analysis.

Despite advancements in ICA morphology classification, the quantitative impact of different ICA geometries on WSS distribution remains underexplored. Given that WSS plays an important role in the initiation of intracranial aneurysms, further investigation is warranted to quantitatively elucidate its relationship with ICA morphology.

To address these challenges, this study applies the above-mentioned classification method to categorize ICA models from the publicly available BraVa dataset [9, 10] into four distinct types—U, V, C, and S—and analyzes their WSS distributions to identify distinct patterns associated with each morphology, emphasizing the role of geometry in shaping local hemodynamics.

2. DATA ACQUISITION

This study utilizes the BraVa open-source dataset, which provides entire cerebral vascular geometry data from 61 healthy individuals. This study focuses on the ICA and the proximal segment of the middle cerebral artery (MCA) before bifurcation, as shown in Figure 1. To account for variations in vessel length and numerical resolution constraints, only 71 cases were selected for further analysis.

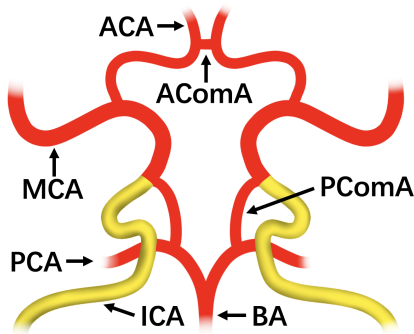


Figure 1. Target region: entire ICA and a portion of MCA prior to MCA bifurcation

The entire cerebral vascular network is extracted into centerline form, and after selecting the target vessels, key parameters such as curvature, torsion, Frenet normals, parallel transport normals, co-

ordinates, and maximum inscribed sphere radius are obtained using V-Modeler [11].

3. CLASSIFICATION METHOD

This study defined ICA shapes using key geometric features, including bend angle (θ), maximum curvature location, superior and inferior extreme points, binormal angle (α), and siphon length, as shown in Fig 2. The UVCS classification follows the scheme illustrated in Fig 3

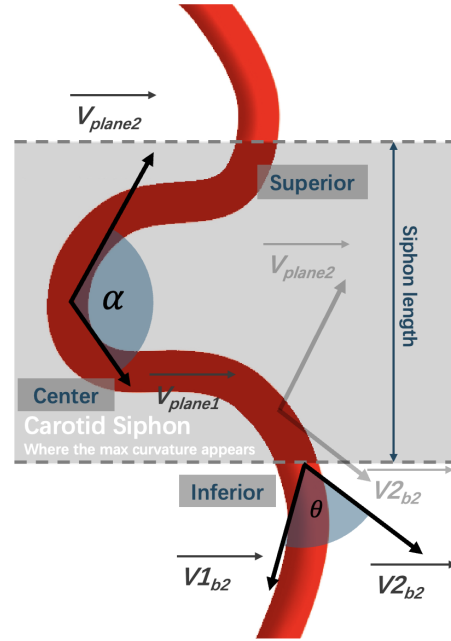


Figure 2. Segmentation of ICA

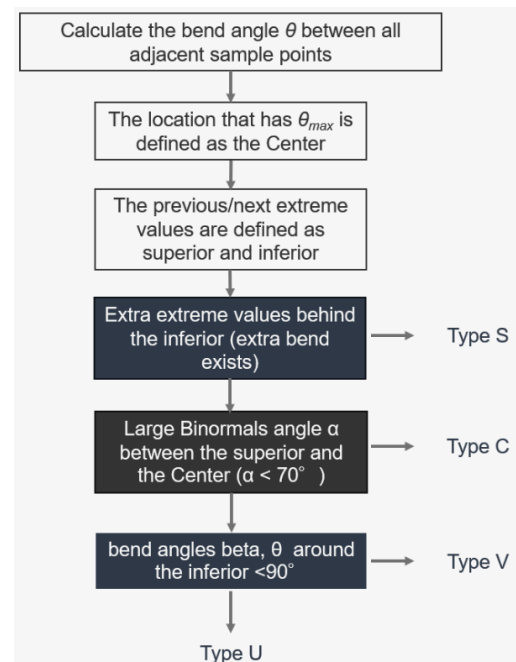


Figure 3. Flowchart of defining the classification

4. 3D MODEL CONSTRUCTION

In this study, the ICA radius was determined based on literature values [12]. Given the significant variation in ICA diameter at different locations— 4.67 ± 0.47 mm in the distal ICA and a 40% reduction (to 2.71 ± 0.37 mm) before entering MCA—a constant radius of 1.5 mm was adopted. This choice ensures a physiologically reasonable vessel morphology while preventing surface overlap in highly curved regions. By maintaining a moderate fixed radius throughout the vascular structure, this study aims to minimize the impact of radius variation on hemodynamic computations while preserving the essential geometric characteristics of the ICA.

The vascular model was reconstructed using Vascular Modeling Toolkit (VMTK) [13], which generates the vessel surface based on the extracted centerline data.

5. NUMERICAL METHOD

The governing equations used in this study follow the incompressible Navier–Stokes framework and are solved using the finite volume method via the open-source CFD platform OpenFOAM (OpenFOAM Foundation, 2024). These equations are expressed as follows:

$$\frac{\partial u_i}{\partial x_i} = 0 \quad (1)$$

$$\frac{\partial u_i}{\partial t} + u_j \frac{\partial u_i}{\partial x_j} = -\frac{1}{\rho} \frac{\partial p}{\partial x_i} + \nu \frac{\partial}{\partial x_j} \left(\frac{\partial u_i}{\partial x_j} + \frac{\partial u_j}{\partial x_i} \right) \quad (2)$$

where u_i , u_j , and x_i , x_j denote the components of velocity and spatial coordinates, respectively.

In this study, we assume that the blood flow is in a steady state, which implies no temporal variation in the velocity field. Based on this assumption, the steady-state solver SimpleFoam was employed to solve the governing equations.

Although blood exhibits shear-thinning non-Newtonian behavior at low shear rates, under high shear conditions typical in large arteries, its viscosity remains nearly constant. Thus, blood was modeled as an incompressible Newtonian fluid with a density of $\rho = 1060$ kg/m³ and a kinematic viscosity of $\nu = 4.43 \times 10^{-6}$ m²/s. Vessel walls were assumed rigid, with no-slip boundary conditions, and viscoelastic effects were neglected.

To reduce numerical artifacts from boundary conditions, inlet and outlet planes were set perpendicular to the vessel centerline and located sufficiently far from the curved region. Computational meshes were generated using ANSYS ICEM CFD software (ANSYS Inc., 2024). Tetrahedral meshes were applied to the vessel lumen, and refined prism layers were constructed near the wall to improve WSS accuracy. Each model comprised approximately 300,000–400,000 elements.

The velocity field was initialized to zero, and the

pressure was uniformly set to 0 Pa. At the inlet, flow rate of 3.63×10^{-6} m³/s was applied, with a zero-gradient pressure boundary condition. At the outlet, the velocity had a zero-gradient condition, and pressure was fixed at 0 Pa as a reference.

6. RESULTS

6.1. Classification Results

Table 1 presents the distribution of UVCS shape classifications in the BraVa dataset. The results indicate that the U-type is the most prevalent, accounting for 42 cases (59.2%), followed by the V-type with 21 cases (29.6%). The C-type comprises 7 cases (9.8%), while the S-type is the least common, with only 1 case (1.4%). These findings suggest that U-type and V-type structures are more frequently observed in the BraVa dataset, whereas C-type and S-type are relatively rare. The distribution pattern is consistent with the proportions reported in the literature.

BraVa		
Type	Count	(Proportion)
U	42	(59.2%)
V	21	(29.6%)
C	7	(9.8%)
S	1	(1.4%)

Table 1. Results of Classification.

6.2. Geometry Comparison and Simulation Results

Four representative UVCS models were selected from the classified BraVa dataset, with the inlet and outlet lengths extended accordingly, as shown in Fig 4.

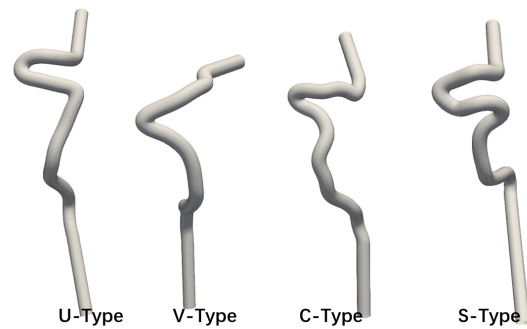


Figure 4. UVCS ICA Model using in CFD

CFD computational meshes were then generated for these models to conduct blood flow simulations. Additionally, the curvature and torsion of the four ICA types were computed, as shown in Fig 5, providing a basis for further exploration of the relationship between geometric characteristics and simulation results.

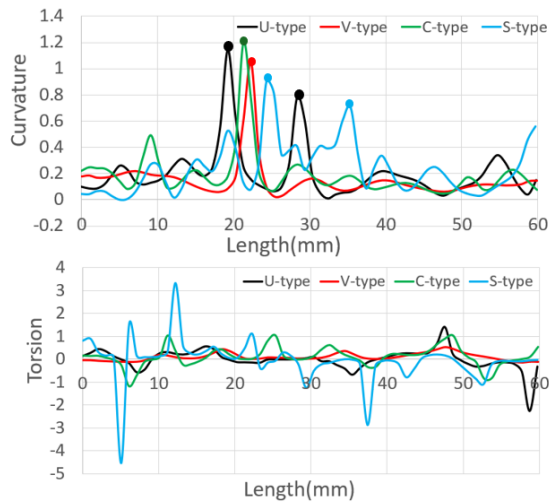


Figure 5. Curvature and Torsion along Centerline

6.2.1. U-type ICA

The U-type vessel is characterized by a distinct curvature in its midsection, forming a U-type configuration. This morphology results in significant bending angles in both the inferior and posterior segments. Additionally, U-type vessels tend to lie within the same plane, indicating a relatively low torsion and a comparatively small alpha angle.

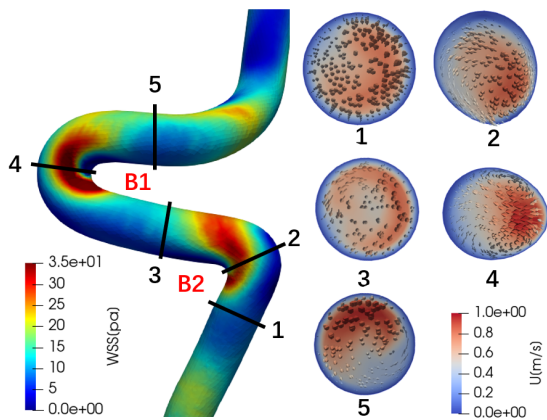


Figure 6. U-type Simulation Result

The curvature pattern of U-type vessels significantly influences blood flow velocity and WSS distribution. As shown in Fig 5, U-type vessels in the ICA siphon region typically exhibit two adjacent curvature peaks, causing rapid flow deviation within the vessel. As illustrated in Fig 6, the first curvature peak directs the main flow toward the outer side of bend B2, while the second curvature peak redirects the flow toward the outer side of bend B1. Consequently, due to these consecutive high-curvature regions, U-type ICAs generally develop two distinct areas of elevated WSS following the bends.

Furthermore, the torsion distribution in Fig 5 in-

dicates that U-type vessels exhibit relatively low torsion peaks, suggesting minimal rotational deformation along the vessel's axis. This implies that U-type vessels primarily undergo planar curvature changes rather than significant spatial twisting, as observed in other vessel types.

6.2.2. V-type ICA

The V-type vessel is characterized by a prominent curvature angle in the ICA siphon region. Compared to U-type vessels, V-type vessels exhibit a more concentrated curvature with fewer bends. The distal bend of the V-type vessel has a relatively smaller curvature angle, and the entire vascular structure primarily lies within a single plane, resulting in a smaller alpha angle.

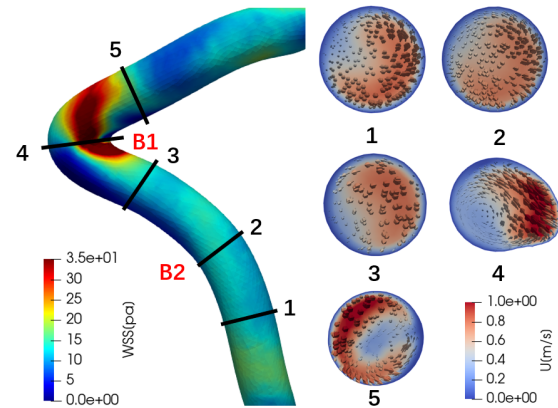


Figure 7. V-type Simulation Result

As shown in Fig 5, V-type ICAs typically exhibit a single major curvature peak in the siphon region. This curvature peak induces significant flow deviation, particularly toward the outer side of bend B1, resulting in a high WSS region, which is noticeably higher than that of U-type vessels, as illustrated in Fig 7. Meanwhile, the central outer region of bend B1 exhibits a low WSS area.

Furthermore, the torsion distribution in Fig 5 indicates that V-type vessels also do not exhibit prominent torsion peaks, suggesting an absence of significant rotational deformation. This implies that V-type vessels primarily exist within the same plane, without noticeable twisting along the vessel's axis.

6.2.3. C-type ICA

The shape of C-type vessels closely resembles that of V-type vessels, they exhibit a distinct feature: a pronounced torsion rate after the center region, particularly near the superior portion. This suggests that C-type vessels do not lie entirely within a single plane and in cases of significant bending, the anterior and posterior segments may be arranged perpendicularly.

As shown in Fig.5, the C-type vascular structures generally share a similar curvature profile with V-type geometries. However, the torsion peaks in

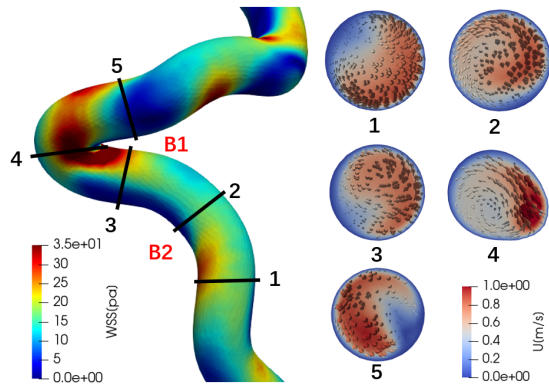


Figure 8. C-type Simulation Result

C-type vessels are significantly higher than those in V-type vessels. Consequently, the elevated torsion after the central portion may induce swirling or eddy formation due to abrupt three-dimensional directional changes in blood flow. In Fig.8, a high WSS region is observed in the high-curvature central portion of the ICA siphon. Additionally, the increased torsion values cause a spatial displacement of the high WSS region in the central part of the ICA siphon. These combined factors contribute to the unique hemodynamic patterns characteristic of the C-type ICA configuration.

6.2.4. S-type ICA

The S-type vascular structure is highly complex, characterized by additional bends appearing before the inferior bend, which further complicates its hemodynamic properties. This vascular configuration is extremely rare in the general population and is scarcely documented in most vascular databases. Consequently, defining the morphological boundaries of S-type vessels remains challenging.

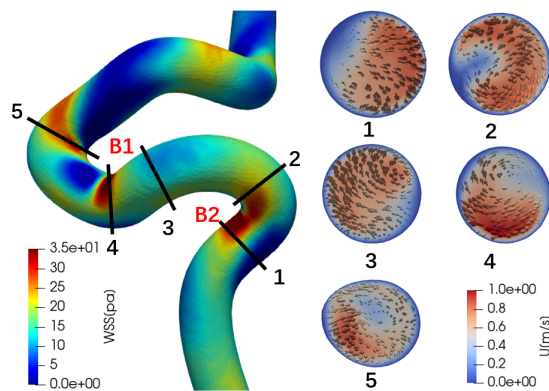


Figure 9. S-type Simulation Result

As observed in Fig 6, the WSS distribution of the S-type vessel is similar to that of the U-type vessel, with two distinct regions of elevated WSS corresponding to the two curvature peaks. In Fig 9, it can be seen that these elevated WSS regions appear

before and after the bends. However, compared to the U-type vessel, the S-type vessel exhibits a greater bending angle at B2, leading to higher WSS values in this region.

Additionally, Fig 5 shows that the torsion distribution of the S-type vessel exhibits greater fluctuations compared to that of the U-type vessel. This increased torsional variation may lead to more swirling or vortex formation, resulting in spatial displacement of WSS and contributing to a more complex flow environment.

7. DISCUSSION

In this study, ICA geometries were classified into four types—U, V, C, and S—based on centerline features. CFD simulations were performed to evaluate WSS distributions for each morphology. The results showed that geometric characteristics such as curvature and torsion were associated with the spatial distribution of high WSS, and that each shape exhibited a characteristic high-WSS pattern.

While this study has demonstrated a relationship between ICA morphology and WSS distribution, several limitations should be noted. The sample models were mainly derived from the BraVa dataset, where S-type geometries were rare, limiting morphological diversity. Additionally, a constant vessel radius was used across all models to control for variability, and patient-specific diameter differences were not considered. Although mesh refinement was applied near the wall, a full mesh independence study remains necessary.

Future work may focus on increasing the number of samples and including pathological cases to enhance the statistical power and clinical relevance of the findings. To improve the objectivity of morphological classification, Principal Component Analysis (PCA) could be applied to uniformly resampled centerline coordinates, allowing for the extraction of dominant shape features and identification of clustering patterns in a reduced-dimensional feature space.

Furthermore, if 3D WSS distributions could be projected onto a two-dimensional representation of the vessel surface, unfolded along the centerline, it would allow for more intuitive and quantitative comparisons across different ICA morphologies. Such a mapping approach may also help clarify how local geometric features influence the distribution of wall shear stress. In addition, machine learning techniques may be applied to predict WSS patterns from geometric input, supporting the development of personalized aneurysm risk assessment models.

8. CONCLUSION

This study classified ICA geometries from the BraVa dataset into four distinct types—U, V, C, and S—and analyzed their impact on WSS distribution using CFD simulations. The results highlight the significant influence of curvature and torsion on WSS, with high-curvature regions exhibiting elev-

ated WSS, which may play a role in vascular remodeling and disease progression.

Among the ICA types, U-type is the most common, characterized by a pronounced midsection curvature, leading to two distinct regions of elevated WSS due to consecutive high-curvature zones. V-type, with a single major curvature peak and fewer bends, exhibits a highly localized high WSS region, particularly at bend B1, with values significantly higher than those in U-type vessels. C-type vessels share a similar curvature distribution with V-type but exhibit significantly higher torsion values. The presence of non-coplanar bends and extreme variations in torsion in C-type vessels leads to a more complex WSS distribution, where high torsion contributes to the spatial displacement of WSS regions. S-type, the least frequent configuration, shares a similar WSS pattern with U-type, featuring two WSS peaks before and after the bends; however, its larger bending angle at B2 results in even higher WSS in that region. Additionally, the greater torsional variation in S-type vessels leads to increased vortex formation and WSS displacement, further complicating the flow environment. These findings emphasize the critical role of ICA morphology in shaping hemodynamic conditions, particularly WSS distribution, which could influence vascular disease risks.

In future research, we can increase the sample size to enhance reliability and further investigate the correlation between shape characteristics and WSS distribution. Establishing this relationship will provide a foundation for the future application of machine learning in predicting WSS distribution based on vascular geometry.

9. ACKNOWLEDGEMENTS

This work was supported by the Fugaku project titled *Development of human digital twins for cerebral circulation using Fugaku*, carried out at the RIKEN Center for Computational Science (Project ID: **hp240220**); as well as by the JSPS KAKENHI grant *Development of an analysis system of systemic-cerebral circulatory metabolism for stroke risk prediction* (Project ID: **22H00190**).

REFERENCES

- [1] Kalaria, R., and Englund, E., 2024, "Neuropathological Features of Cerebrovascular Diseases", *Pathology*.
- [2] Brisman, J. L., Song, J. K., and Newell, D. W., 2006, "Cerebral Aneurysms", *New England Journal of Medicine*, Vol. 355 (9), pp. 928–939.
- [3] Muthukumar, K., Moses, V., Keshava, S. N., and Padmanabhan, A., 2021, "Inadvertent Intraprocedural Complication of a Flow Diverter Device During Treatment of Internal Carotid Artery Aneurysm: A Case Report", *Vascular Disease Management*, Vol. 18 (8), pp. E139–E143.
- [4] Meng, H., Meng, H., Xiang, J., and Siddiqui, A. M., 2013, "High WSS or Low WSS? Complex Interactions of Hemodynamics with Intracranial Aneurysm Initiation, Growth, and Rupture: Toward a Unifying Hypothesis", *Stroke*, Vol. 35 (7), pp. 1254–1262.
- [5] Metaxa, E., Tremmel, M., Natarajan, S. K., Xiang, J., Paluch, R. A., Mandelbaum, M., Siddiqui, A. H., Kolega, J., Mocco, J., and Meng, H., 2010, "Characterization of Critical Hemodynamics Contributing to Aneurysmal Remodeling at the Basilar Terminus in a Rabbit Model", *Stroke*, Vol. 41 (8), pp. 1774–1782.
- [6] Lauric, A., Hippelheuser, J., Safain, M. G., and Malek, A. M., 2014, "Curvature Effect on Hemodynamic Conditions at the Inner Bend of the Carotid Siphon and Its Relation to Aneurysm Formation", *Stroke*, Vol. 47 (12), pp. 3018–3027.
- [7] Zhang, C., Pu, F., Li, S., Xie, S. Q., Fan, Y., and Li, D., 2012, "Geometric Classification of the Carotid Siphon: Association Between Geometry and Stenoses", *International Journal of Cardiovascular Imaging*, Vol. 35 (5), pp. 385–394.
- [8] Sangalli, L. M., Secchi, P., Vantini, S., et al., 2010, "K-mean alignment for curve clustering", *Computational Statistics & Data Analysis*, Vol. 54, pp. 1219–1233.
- [9] Wright, S. N., Kochunov, P., Bergamino, F. M. M., Brown, K. M., Mazziotta, J. C., Toga, A. W., Cebal, J. R., and Ascoli, G. A., 2013, "Digital Reconstruction and Morphometric Analysis of Human Brain Arterial Vasculature from Magnetic Resonance Angiography", *NeuroImage*, Vol. 82, pp. 170–181, URL <http://dx.doi.org/10.1016/j.neuroimage.2013.05.089>.
- [10] Center for Neural Informatics, Krasnow Institute for Advanced Study, George Mason University, 2013, "BRAVA - Brain Arterial Vascular Atlas", Available at <http://cng.gmu.edu/brava>.
- [11] Kobayashi, M., Hoshina, K., Yamamoto, S., Nemoto, Y., Akai, T., Shigematsu, K., Watanabe, T., and Ohshima, M., 2015, "Development of an Image-Based Modeling System to Investigate Evolutional Geometric Changes of a Stent Graft in an Abdominal Aortic Aneurysm", *Circulation Journal*, Vol. 79 (7), pp. 1534–1541.
- [12] Baz, R. A., Scheau, C., Niscoveanu, C., and Bordei, P., 2021, "Morphometry of the Entire Internal Carotid Artery on CT Angiography", *Medicina*, Vol. 57 (8), p. 832.

- [13] Izzo, R., Steinman, D., Manini, S., and Antiga, L., 2018, “The Vascular Modeling Toolkit: A Python Library for the Analysis of Tubular Structures in Medical Images”, *Journal of Open Source Software*, Vol. 3 (25), p. 745.